Radiological Physics and Technology (2019) 12:149–155
https://doi.org/10.1007/s12194-019-00501-1

Voxel-based morphometry analysis of double inversion-recovery magnetic resonance imaging for detecting microscopic lesions: a simulation study

Sato Yusuke[1] · Hayashi Norio[2] · Maruyama Tomoko[1] · Motegi Shunichi[3] · Ujita Koichi[4] · Suto Takayuki[4] · Watanabe Haruyuki[2] · Ogura Toshihiro[2] · Ogura Akio[2] · Tsushima Yoshito[5]

Received: 20 July 2018 / Revised: 6 February 2019 / Accepted: 11 February 2019 / Published online: 22 February 2019

Abstract
Double inversion-recovery (DIR) imaging has the potential to improve the detection of subcortical lesions through the use of voxel-based morphometry (VBM) analysis. The aim of this study was to clarify the characteristics of detectable lesions by performing a VBM analysis on DIR images of simulated lesions. Twenty healthy volunteers underwent magnetic resonance imaging using a head three-dimensional DIR sequence. The images were processed using SPM12; then, the selected images with simulated lesions were analyzed via VBM. The VBM results were evaluated using free-response receiver-operating characteristic curves and a receiver-operating characteristic analysis. The sensitivity was 100% (5/5), with 5.6 false-positive objects per case, in simulated lesions with a contrast of 0.6 and a size of 2.4 mm. The sensitivity was 80% (4/5), with 5.4 false-positive objects per case, in simulated lesions with a contrast of 0.5 and a size of 2.4 mm. The mean area under the curve value was increased from 0.783 to 0.883 using VBM, with a statistically significant difference ($p < 0.01$). The VBM analysis of the DIR images using SPM alone showed the potential to detect subcortical microscopic lesions. Early detection of Alzheimer's disease may be possible by adapting VBM in the clinical setting.

Keywords MRI · DIR · SPM · VBM

1 Introduction

Detection of cortical microinfarction is useful in the early detection of Alzheimer's disease, as several neuropathological studies have shown an association between Alzheimer's disease and microinfarction [1]. However, microinfarcts cannot be detected by conventional magnetic resonance imaging (MRI) because of their small sizes. However, since the introduction of ultrahigh field strength (7.0 T) magnetic resonance (MR) scanners, which offer higher spatial resolution, in vivo detection of microinfarcts may be possible [1]. Moreover, microinfarcts can be detected with regular clinical MR scanners (3.0 T) that use a double inversion-recovery (DIR) sequence [2]. It is possible to suppress two different tissue types using two inversion pulses within a DIR sequence. White matter-attenuated inversion-recovery (WAIR) images, in which white matter (WM) and cerebrospinal fluid (CSF) are suppressed and gray matter (GM) is emphasized, are useful in the visualization of GM. Thus, these imaging modalities are important for the diagnosis and management of many neurological diseases, including schizophrenia, multiple sclerosis, stroke, Alzheimer's disease, tuberous sclerosis, and epilepsy, all of which are associated with changes in cortical GM [3]. However, cortical microinfarcts appearing as small and pale high-signal lesions on GM are difficult to detect, because GM exhibits a thin, complicated,

✉ Sato Yusuke
mr175101@gchs.ac.jp

1 Department of Radiological Technology, Graduate School of Radiological Technology, Gunma Prefectural College of Health Sciences, 323-1 Kamioki, Maebashi, Gunma 371-0052, Japan

2 Department of Radiological Technology, Gunma Prefectural College of Health Sciences, Maebashi, Japan

3 Department of Radiology, Josai Clinic, Maebashi, Japan

4 Department of Radiology, Gunma University Hospital, Maebashi, Japan

5 Department of Diagnostic Radiology and Nuclear Medicine, Gunma University Graduate School of Medicine, Maebashi, Japan

convoluted structure, whereas DIR images exhibit a low spatial resolution.

Voxel-based morphometry (VBM) is widely used for the analysis of brain MR images. Notably, VBM is an automatic quantitative volumetric technique that analyzes the entire brain through voxel-by-voxel analysis; this method is objective and sensitive, has good reproducibility, and is suitable for the detection of subtle brain structural changes that precede more obvious brain volume loss on conventional MRI [4]. In the usual VBM, voxel-based analysis is used to detect brain atrophy by registering each brain morphology to the standard brain space (spatial normalization). This makes quantitative evaluation of the brain volume changes possible; a voxel with an abnormal signal intensity for the control group could not be recognized in the original images by processing spatial normalization. VBM is useful for a wide range of applications, including the identification of cortical atrophy sites in degenerative diseases and the detection of lesion sites in cases of multiple sclerosis or stroke [4–9]. The brain volumes in the lesion and atrophic sites are changed. Identification of atrophy is synonymous with detection of the lesions in that the voxel presenting an abnormal signal intensity is detected. In addition, VBM is useful for analysis of a single subject. In the Voxel-Based Specific Regional Analysis System for Alzheimer's Disease, single-subject data are compared with those of the control group by applying the VBM technique [5, 10]. Therefore, applying VBM to DIR images is expected to improve the sensitivity of the detection of subcortical lesions. However, no reports have indicated the application of VBM to DIR images, nor has an appropriate analysis method been established. Therefore, the aim of our study was to clarify the characteristics of detectable lesions by performing a VBM analysis for DIR images generated through the use of simulated lesions.

2 Materials and methods

2.1 Acquisition of MRI scans

Twenty healthy volunteers (6 women and 14 men; mean age 23.5 ± 5.0 years; age range 21–39 years) underwent MRI (Ingenia 1.5 T, Philips, Amsterdam, The Netherlands) with a head three-dimensional (3-D) DIR sequence (repetition time = 8000 ms, echo time = 73 ms, inversion time (TI)-first = 2630 ms, TI-second = 372 ms, field of view = 240 × 240 mm, matrix = 240 × 240, slice thickness = 2 mm, and slice interval = 1 mm). This study was approved by our institutional review board, and volunteers provided written informed consent prior to participation.

2.2 VBM system

All analyses were performed using Statistical Parametric Mapping 12 (SPM12; Wellcome Department of Imaging Neuroscience, London, UK), which operates on MATLAB R2016b (Mathworks, Natick, MA, USA). Two VBM systems were compared to develop a system suitable for the detection of high-signal-intensity cortical lesions on DIR images.

The first VBM system consisted of the following four preprocesses: segmentation, spatial normalization, smoothing, and statistical analysis. All processes were conducted with the standard SPM12 settings. In the segmentation procedure, brain structure images were classified into GM, WM, and CSF images. In this study, we targeted cortical lesions; thus, subsequent processing was performed only on GM images. In the normalization procedure, the GM images of each subject were registered to a standard Montreal Neurological Institute (MNI) space to correct differences in the shape of each subject's brain. For the normalization procedure, we used the DARTEL technique, which provides a more accurate transformation within the MNI space than a conventional normalization algorithm [11]. In the smoothing procedure, a Gaussian kernel filter was used to smooth normalized images, thereby absorbing individual differences that could not be eliminated by spatial normalization. The kernel size of the Gaussian filter was set to 8 mm in full-width at half-maximum (FWHM). In the statistical analysis, a two-sample *t* test was applied to compare the images of healthy subjects to images containing a simulated lesion. The region with increased brain volume was analyzed, because the simulated lesions have high-signal intensity.

The preprocess of the second VBM system consisted only of spatial normalization to prevent mis-segmentation of the lesion sites. The normalization procedure was performed without the use of DARTEL, because the segmentation procedure was omitted. In addition, the smoothing procedure was omitted to improve sensitivity. Statistical analysis was performed in the same manner as in the first VBM system.

2.3 Simulated lesions

A probability density function consisting of the *p*-dimensional normal distribution given by Eq. (1) was used to create simulated lesions:

$$f(x_1, x_2 \ldots x_p|\mu,\ \Sigma) = \frac{1}{\sqrt{|\Sigma|(2\pi)^p}} \exp\left\{-\frac{1}{2}(x-\mu)\Sigma^{-1}(x-\mu)'\right\}$$

$$\mu = \begin{bmatrix} \mu_1 \\ \mu_2 \\ \vdots \\ \mu_p \end{bmatrix}, \quad \Sigma = \begin{bmatrix} \sigma_1^2 & \sigma_{12} & \cdots & \sigma_{1p} \\ \sigma_{21} & \sigma_2^2 & \cdots & \sigma_{2p} \\ \vdots & \vdots & & \\ \sigma_{p1} & \sigma_{p2} & & \sigma_p^2 \end{bmatrix}, \tag{1}$$

where μ is the expected value of probability variable x and σ is the standard deviation of variable x. In this study, simulated lesions were created by adding a probability density function consisting of a 3D normal distribution. Simulated lesions were added to the same position on the GM based on anatomical structure to eliminate the influence of position difference. The central coordinate of the simulated lesion was changed by adjusting the expected value μ. The size of the simulated lesions was changed by adjusting the standard deviation σ of the normal distribution. The diagonal and off-diagonal elements of the covariance matrix were set to zero to create spherical simulated lesions. The diameter of the simulated lesions is calculated using Eq. (2):

$$\mathrm{FWHM} = 2\sigma\sqrt{2\log_e 2}\,(\mathrm{mm}). \tag{2}$$

Each voxel value of the simulated lesion $V_n(x_1, x_2, x_3)$ was calculated with Eq. (3):

$$V_n(x_1, x_2, x_3) = a \cdot (f_{\max}/f(x_1, x_2, x_3)), \tag{3}$$

where a is the arbitrary weighting factor and $f_{\max}$ is the maximum value of function x. The voxel value of the simulated lesion was changed by adjusting the weighting factor a, and the maximum value of $V_n(x_1, x_2, x_3)$ was used as the signal intensity of the simulated lesion. The contrast representing differences between the signal intensity of the simulated lesion ($\mathrm{SI_{SL}}$) and the signal intensity of GM ($\mathrm{SI_{GM}}$) was calculated with Eq. (4):

$$\mathrm{Contrast} = \left|\mathrm{SI_{SL}} - \mathrm{SI_{GM}}\right| / \left|\mathrm{SI_{SL}} + \mathrm{SI_{GM}}\right|. \tag{4}$$

For comparison of the sensitivity of detection between the two VBM systems, we created a large simulated lesion with high-signal intensity. The standard deviation of the normal distribution was set to 10, and the weighting factor a was set to 100. Thus, the size of the simulated lesions was 24 mm in FWHM, and the contrast with GM was 0.5. An image adding simulated lesions was selected randomly from 20 healthy subjects. The remaining 19 images were used as the control group. An image containing simulated lesions was analyzed using both VBM systems. This procedure was repeated five times by changing the image by adding the simulated lesion.

In addition, we investigated smaller simulated lesions using a VBM system that showed high sensitivity. The standard deviation was set to 1 or 2 (with a size of 2.4 or 4.7 mm in FWHM), and the weighting factor was set to 150, 100, and 70 (with a contrast of 0.6, 0.5, or 0.4 with GM). Similarly, images containing simulated lesions were analyzed with VBM.

2.4 Evaluation

To compare the two VBM systems, the sensitivity of the detection of the large stimulated lesions was visually evaluated using output images from each VBM analysis. The additional investigation was physically and visually evaluated. The physical evaluation was conducted to clarify the condition of detectable lesions using VBM. The p values ranged from 0.001 to 0.05 (8 points); the sensitivity and number of false positives were determined for each condition on the basis of the analysis results and then evaluated using free-response receiver-operating characteristic (FROC) curves. We defined the detection of simulated lesions when lesions were observed as a region with high-signal intensity on the t-value map. False-positive objects were counted only within the brain. The visual evaluation was conducted to compare the performance between original DIR images and the VBM results. The observers' performance in the detection of simulated lesions without and with the VBM results was evaluated using receiver-operating characteristic (ROC) analysis. Three radiological technologists participated in the observer performance test. The data set consisted of 20 normal DIR images, 20 DIR images containing a simulated lesion, and the VBM results of the same slice section corresponding to original DIR images. DIR images were converted from DICOM format to 8-bit images. The window width and level were fixed to appropriate values. The viewing time was not limited in this study. Before the test, each observer underwent sufficient training to understand the test procedure and characteristics of the DIR images and VBM. The procedure of the observer test consisted of the following four processes: (1) the original DIR image was displayed on a medical imaging monitor; (2) each observer rated the confidence level in the presence or absence of a simulated lesion using a continuous rating scale; (3) the VBM result was displayed next to the original DIR image; and (4) the observer viewed both the original DIR image and the VBM result, and rated them again. The ROC curves from the continuous rating data were obtained using a computer program (ROCKIT 0.9B; C. E. Metz, University of Chicago, Chicago, IL, USA). The statistical significance of the difference in areas under the curve (AUC) obtained with and without VBM was tested using a paired Student t test.

3 Results

Figure 1 shows DIR images with added simulated lesions (size, 24 mm; contrast, 0.5), alongside preprocessed images. Simulated lesions were observed on preprocessed images as regions with high-signal intensity when using the second VBM system. However, lesions were not observed on preprocessed images when using the first VBM system. Figure 2 shows the results of the VBM analysis. The brain region with the added simulated lesion was observed as a region with high-signal intensity on the t value map in the second VBM system; however, the lesion was not observed on the t value map in the first VBM system. The sensitivity

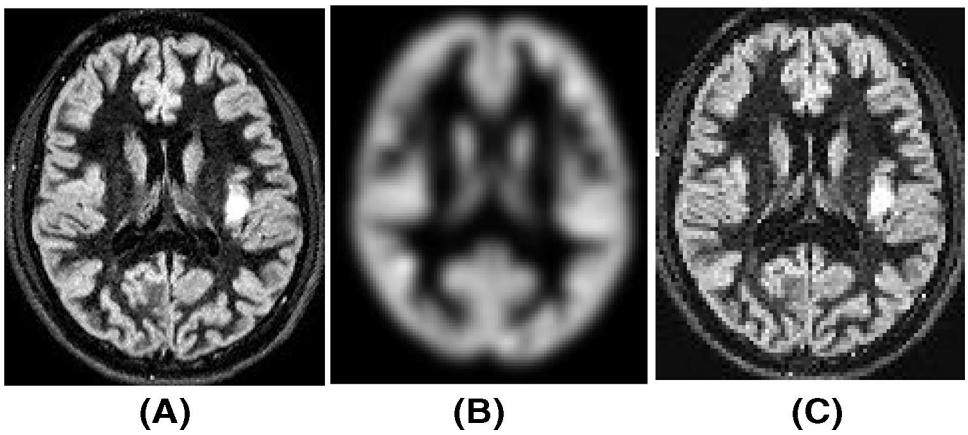

Fig. 1 **a** A representative double inversion-recovery (DIR) image with an added simulated lesion. The size of the simulated lesion was set to 24 mm in full-width at half-maximum (FWHM), and the contrast with gray matter (GM) was set to 0.5. **b** A representative preprocessed image generated using the first voxel-based morphometry (VBM) system. **c** A representative preprocessed image generated using the second VBM system. The simulated lesion was only observed in **c**

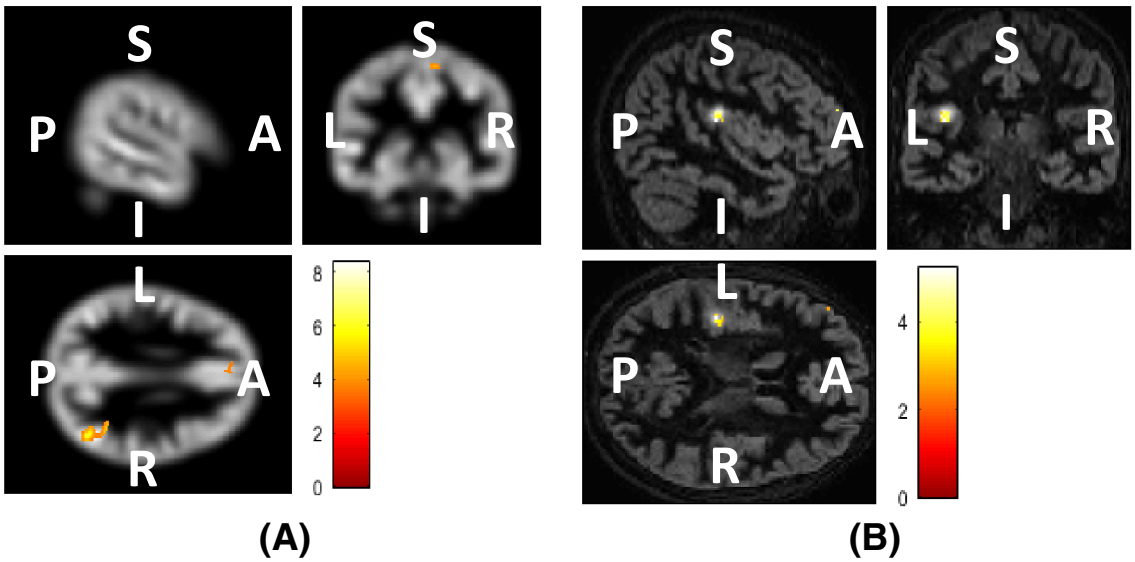

Fig. 2 **a** A representative result of the voxel-based morphometry (VBM) analysis, generated using the first VBM analysis method, whereas **b** is a representative result of the VBM analysis, generated using the second VBM analysis method. The brain region with the added simulated lesions corresponded to a high-signal-intensity region of the *t* value map only in **b**, whereas the false-positive objects can be observed in **a**

for the detection of lesions was 20% (1/5) with the first VBM system and 100% (5/5) with the second VBM system.

We conducted additional investigations with the second VBM system, as it demonstrated high sensitivity. Figure 3 shows the results of the DIR images that had been modified with smaller simulated lesions. Figure 4 shows the VBM results; the brain region containing the simulated lesions corresponded to a high-signal-intensity region on the *t* value map. Figure 5 shows the FROC curves generated with the results of the VBM analysis of five cases. The sensitivity was 100% (5/5), with 5.6 false-positive objects per case, in the simulated lesions with a contrast of 0.6 and a size of 2.4 mm; 80% (4/5), with 5.4 false-positive objects per case, in simulated lesions with a contrast of 0.5 and a size of 2.4 mm; and 80% (4/5), with 7.6 false-positive objects per case, in simulated lesions with a contrast of 0.4 and a size of 4.7 mm. Figure 6 shows the mean ROC curves for the three observers in the detection of high-signal-intensity simulated lesions from the DIR images with and without the VBM result. The mean AUC value was increased from 0.783 to 0.883 when the observers viewed both the original DIR images and the VBM result, and the difference was statistically significant ($p < 0.01$).

4 Discussion

In a comparison of the sensitivity of detection for simulated lesions, the second VBM system (without DARTEL) exhibited higher sensitivity than the first VBM system

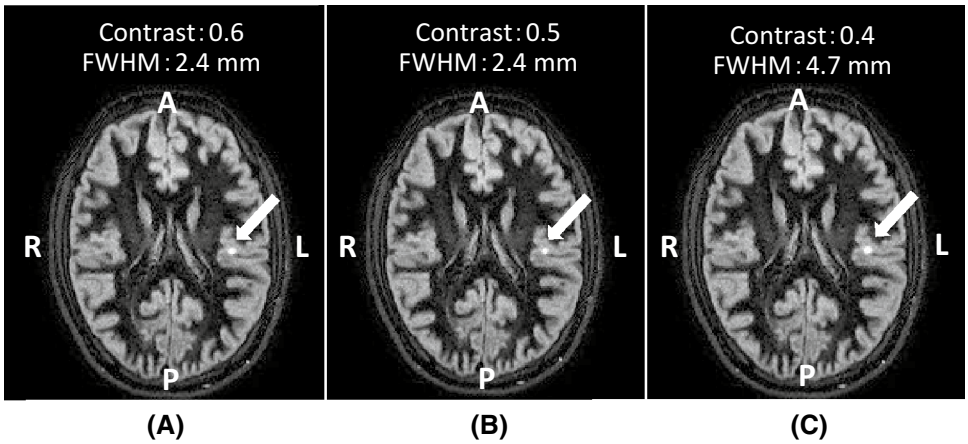

Fig. 3 Double inversion-recovery (DIR) images with added simulated lesions. The lesion in **a** was 2.4 mm in size, with a contrast of 0.6. The lesion in **b** was 2.4 mm in size, with a contrast of 0.5. The lesion in **c** was 4.7 mm in size, with a contrast of 0.6

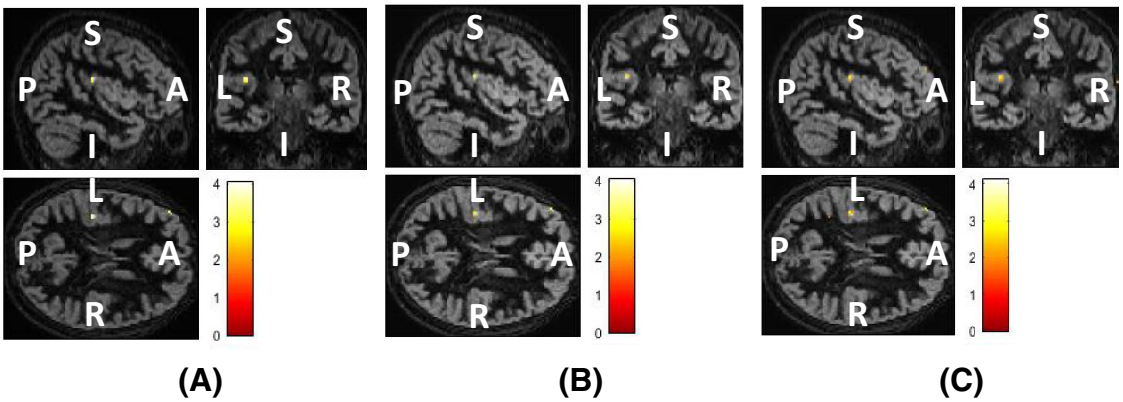

Fig. 4 Results of the voxel-based morphometry (VBM) analysis with the second analysis method. The brain regions with added simulated lesions each corresponded to a region with high-signal intensity on the *t* value maps in **a, b**, and **c**

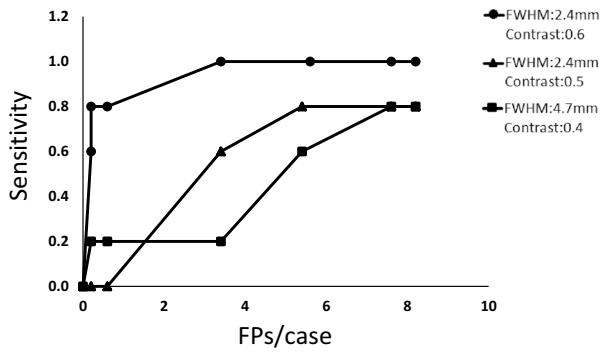

Fig. 5 Free-response receiver-operating characteristic (FROC) curves created by assessing the results of the voxel-based morphometry (VBM) analysis in five cases. The sensitivity was 100% (5/5), with 5.6 false-positive objects per case, in simulated lesions with a contrast of 0.6 and a size of 2.4 mm; 80% (4/5), with 5.4 false-positive objects per case, in simulated lesions with a contrast of 0.5 and a size of 2.4 mm; and 80% (4/5), with 7.6 false-positive objects per case, in simulated lesions with a contrast of 0.4 and a size of 4.7 mm

(with DARTEL). Thus, we conducted a VBM analysis of the DIR images with the second VBM system. The minimum detectable lesion size was 2.4 mm when the contrast was 0.6 or 0.5. As the contrast of the simulated lesion decreased, the minimum detectable lesion size increased; when the contrast of the lesion was 0.4, the minimum detectable lesion size was 4.7 mm. The result of the ROC analysis showed that the detectability of simulated lesions was significantly improved using VBM. Therefore, our proposed method is useful for improving the detectability of cortical microscopic lesions on DIR images.

Many studies have utilized VBM with DARTEL, confirming the usefulness of DARTEL [4, 5, 11]. In general, the analysis accuracy of VBM with DARTEL is improved when T1-weighted images are used. However, when DARTEL was applied in the DIR images in this study, the sensitivity for lesion detection was reduced, which may be a result of the errors in the segmentation procedure.

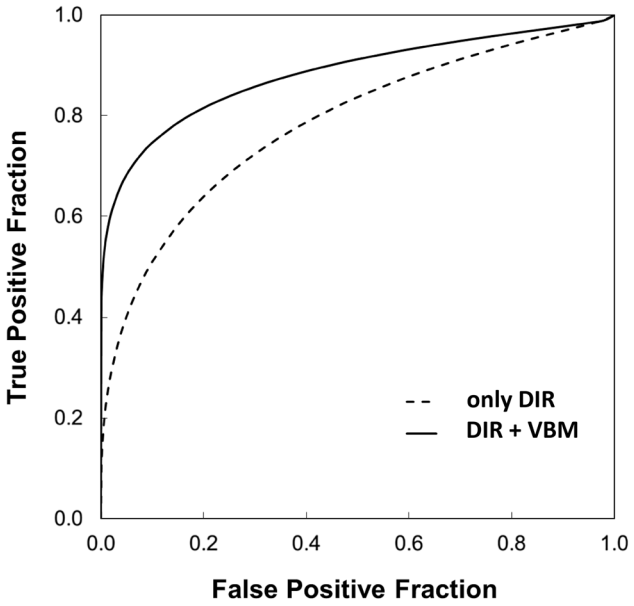

Fig. 6 Mean receiver-operating characteristic (ROC) curves for the three observers in the detection of high-signal-intensity simulated lesions from the double inversion-recovery (DIR) images without and with the result of voxel-based morphometry (VBM). The mean area under the curve (AUC) was increased from 0.783 to 0.883 when the observers viewed both the original DIR images and the VBM result, with a statistically significant difference ($p < 0.01$)

Figure 7 shows the results of the segmentation procedure of DIR images with an added simulated lesion using the first VBM system. The brain regions with additional simulated lesions were observed as a region with low signal intensity in two cases. In the other three cases, the regions were segmented as a normal GM. On the basis of this result, we analyzed the region with decreased brain volume. However, the sensitivity for the detection of lesions was 0% (0/5). As the brain region with the additional simulated lesions could not be classified correctly, the trace of the lesion was not reflected in the preprocessed images. Therefore, the lesions could not be detected in the first VBM system, which used DARTEL. Although DARTEL is a useful technique to improve the accuracy of a special normalization procedure, it must be combined with the segmentation procedure in SPM12. DARTEL cannot be used while omitting the segmentation procedure. Therefore, the use of the segmentation procedure is not recommended to detect lesions of DIR images by VBM. By contrast, simulated lesions were detected with the second VBM system, which consisted of only SPM12 spatial normalization, without DARTEL. The VBM system that we describe here may improve the diagnostic sensitivity for many neurological diseases that are represented by DIR images.

DIR images are useful to detect cortical microinfarcts found in the early stages of Alzheimer's disease [2];

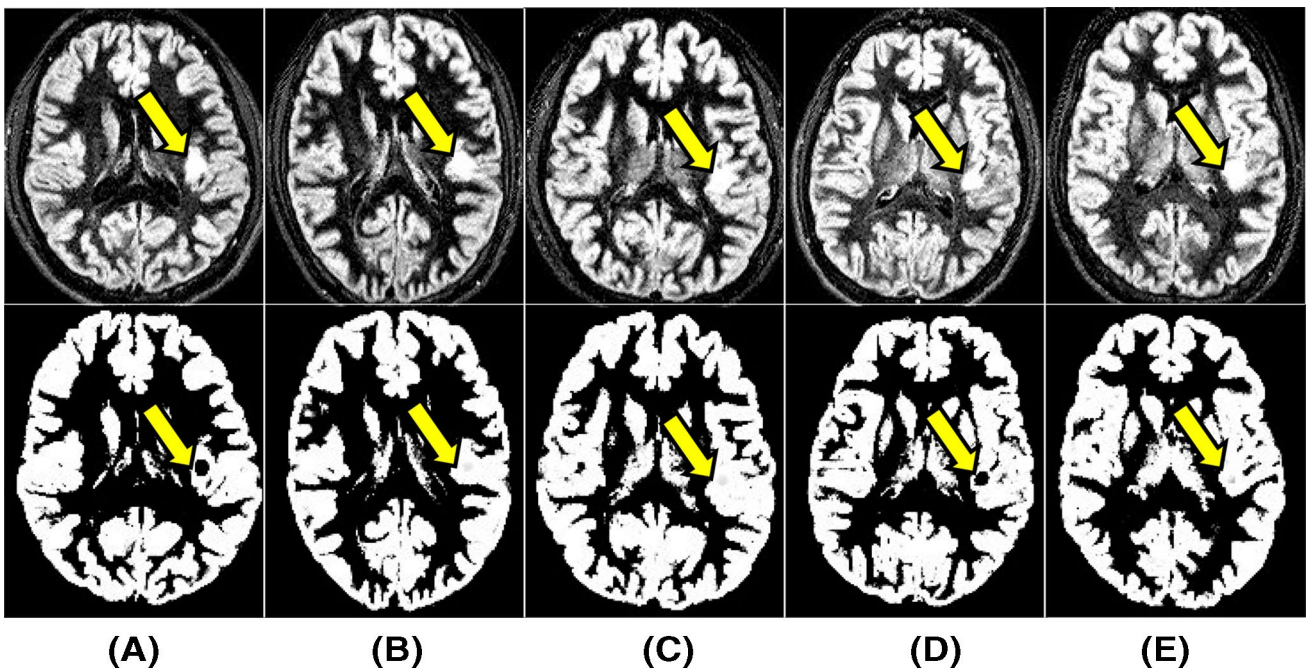

Fig. 7 Upper five images indicate the original double inversion-recovery (DIR) images with a simulated lesion. The lower five images show the results of the segmentation procedure of the upper figures using the first voxel-based morphometry (VBM) system. The brain regions with a simulated lesion (arrows) were observed as a region with low signal intensity in two cases (**a, d**). In the other three cases, the regions were segmented as a normal gray matter (**b, c, e**)

importantly, the sizes of these cortical microinfarcts are range from 0.05 to 5 mm [12]. The use of VBM can quantitatively evaluate lesions by statistical analysis. To evaluate the minimum size of lesions detectable by VBM, we utilized a size of 2.4 mm for high-contrast lesions and 4.7 mm for low-contrast lesions. Our results suggest that the VBM system can detect relatively large cortical microinfarcts. In addition, the results of the observer performance test showed that the use of VBM could significantly improve the confidence levels in identifying the existence of simulated cortical lesions. This result indicates that the radiologist's performance in the detection of microscopic cortical lesions was improved and the misinterpretation of these lesions was reduced. Thus, we believe that our proposed method could contribute to improve the accuracy for the detection of cortical microinfarcts. Moreover, DIR images are also useful for the representation of WM lesions such as multiple sclerosis [13]. As our proposed method can provide quantitative evaluation of WM and GM, the diagnostic accuracy for WM and GM lesions is expected. Thus, VBM may be useful for the detection of WM diseases.

Our study has several limitations. First, this was a simulation study using images from healthy subjects that were modified by the addition of simulated lesions. Second, the sizes and contrasts of the lesions were examined, but not their positions. In addition, the sensitivities for the detection of real lesions were not evaluated. Therefore, we plan to evaluate clinical images present in the current clinical findings. Moreover, a brain template for DIR images is not available in the current version of the SPM software. In the future, the accuracy of VBM for analysis of DIR images may be improved if a brain template for DIR images is created.

5 Conclusion

We compared the abilities of two VBM systems to detect subcortical lesions present on DIR images. The sensitivity of detection of the VBM system that consisted only of spatial normalization was markedly higher than that of the VBM system that utilized DARTEL. Thus, the sensitivity for detection of microscopic lesions such as cortical microinfarcts can be improved using this VBM system. Furthermore, early detection of Alzheimer's disease may be possible by adapting VBM in the clinical setting.

Compliance with ethical standards

Conflict of interest The authors declare that they no conflicts of interest.

Statement of human rights All procedures performed in studies involving human participants were in accordance with the ethical standards of the institutional research committee and with the 1964 Helsinki Declaration and its later amendments or comparable ethical standards.

Statements of animal rights This article does not contain any animal studies performed by any of the authors.

Informed consent Informed consent was obtained from all individual participants included in this study.

References

1. Brundel M, de Bresser J, van Dillen JJ, Kappelle LJ, Biessels GJ. Cerebral microinfarcts: a systematic review of neuropathological studies. J Cereb Blood Flow Metab. 2012;32(3):425–36.
2. Ii Y, Maeda M, Kida H, Matsuo K, Shindo A, Taniguchi A, et al. In vivo detection of cortical microinfarcts on ultrahigh-field MRI. J Neuroimaging. 2013;23(1):28–32.
3. Boulby PA, Symms MR, Barker GJ. Optimized interleaved whole-brain 3D double inversion recovery (DIR) sequence for imaging the neocortex. Magn Reson Med. 2004;51(6):1181–6.
4. Chen Z, Li L, Sun J, Ma L. Mapping the brain in type II diabetes: voxel-based morphometry using DARTEL. Eur J Radiol. 2012;81(8):1870–6.
5. Matsuda H, Mizumura S, Nemoto K, Yamashita F, Imabayashi E, Sato N, et al. Automatic voxel-based morphometry of structural MRI by SPM8 plus diffeomorphic anatomic registration through exponentiated lie algebra improves the diagnosis of probable Alzheimer disease. Am J Neuroradiol. 2012;33(6):1109–14.
6. Schmidt P, Gaser C, Arsic M, Buck D, Forschler A, Berthele A, et al. An automated tool for detection of FLAIR-hyperintense white-matter lesions in multiple sclerosis. Neuroimage. 2012;59(4):3774–83.
7. Shigemoto Y, Matsuda H, Kamiya K, Maikusa N, Nakata Y, Ito K, et al. In vivo evaluation of gray and white matter volume loss in the parkinsonian variant of multiple system atrophy using SPM8 plus DARTEL for VBM. Neuroimage Clin. 2013;2:491–6.
8. Spies L, Tewes A, Suppa P, Opfer R, Buchert R, Winkler G, et al. Fully automatic detection of deep white matter T1 hypointense lesions in multiple sclerosis. Phys Med Biol. 2013;7;58(23):8323–37.
9. Takahashi N, Tsai DY, Lee Y, Kinoshita T, Ishii K. *Z*-score mapping method for extracting hypoattenuation areas of hyperacute stroke in unenhanced CT. Acad Radiol. 2010;17(1):84–92.
10. Nakatsuka T, Imabayashi E, Matsuda H, Sakakibara R, Inaoka T, Terada H. Discrimination of dementia with Lewy bodies from Alzheimer's disease using voxel-based morphometry of white matter by statistical parametric mapping 8 plus diffeomorphic anatomic registration through exponentiated Lie algebra. Neuroradiology. 2013;55(5):559–66.
11. Klein A, Andersson J, Ardekani BA, Ashburner J, Avants B, Chiang MC, et al. Evaluation of 14 nonlinear deformation algorithms applied to human brain MRI registration. Neuroimage. 2009;46(3)(1):786–802.
12. van Dalen JW, Scuric EE, van Veluw SJ, Caan MW, Nederveen AJ, Biessels GJ, et al. Cortical microinfarcts detected in vivo on 3 T MRI: clinical and radiological correlates. Stroke. 2015;46(1):255–7.
13. Simon B, Schmidt S, Lukas C, Gieseke J, Traber F, Knol DL, et al. Improved in vivo detection of cortical lesions in multiple sclerosis using double inversion recovery MR imaging at 3 T. Eur Radiol. 2010;20(7):1675–83.